Fourier plane colorimetric sensing using broadband imaging of surface plasmons and application to biosensing

P. Arora and A. Krishnan'

Articles you may be interested in

Fabrication of tunable plasmonic substrates using a table-top gold coater and a hot plate, their optical characterization, and surface enhanced Raman activity
118, 154901154901 (2015); 10.1063/1.4933283

Fourier plane colorimetric sensing using broadband imaging of surface plasmons and application to biosensing

P. Arora[1,2] and A. Krishnan[1,2,a)]

[1]*Centre for NEMS and Nano Photonics (CNNP), Department of Electrical Engineering, Indian Institute of Technology Madras, Chennai-600036, India*
[2]*Experimental Optics Laboratory, Department of Electrical Engineering, Indian Institute of Technology Madras, Chennai-600036, India*

We demonstrate an optical technique for refractive index and thickness sensing of sub-wavelength-thick dielectric analytes. The technique utilizes the broadband, multimode, directional leakage radiation arising from the excitation of hybrid mode surface plasmons (SP) on low aspect ratio periodic plasmonic substrates with period $\approx \lambda$. The approach requires relaxed fabrication tolerances compared to extra ordinary transmission-based sensing techniques, wherein minor shifts in the fabricated dimensions result in a very large change from the designed resonant wavelength. We show that refractive index perturbations due to about 10-nm-thick dielectric can be captured optically by the usage of carefully designed plasmonic substrates, a halogen lamp source, free-space optical components, polarizers, and a low-end, consumer-grade charge coupled device camera. The plasmonic substrates were designed for converting the signature of hybrid mode SP excitation into a transmission peak by utilizing a thin homogeneous metal layer sandwiched between the periodic plasmonic structures and the substrate. The resonance is highly sensitive to the refractive index and thickness of the analyte superstrate. The excitation of hybrid mode SP results in a polarization rotation of 90° of the leaked radiation at resonant wavelength. In order to eliminate the problem of image registration (i.e., placing the same feature in the same pixel of the image, for comparison before and after a change in refractive index) for sensing, we perform the color analysis in the Fourier plane. The change in color of the bright emitted spot with highest momentum, corresponding to the leakage of fundamental SP mode, was used to measure the changes in refractive index, whereas the number and color of spots of lower momenta, corresponding to higher-order Fabry Perot modes, was used to measure the variation in thickness. We further show that the Fourier plane analysis can also be used to sense the index of thicker dielectrics, where real plane image analysis may fail to sense index perturbations, simply due to superposition of different modes in the real plane images of such substrates. Control experiments and analysis revealed a refractive index resolution of 10^{-5} RIU. The results were correlated with simulations to establish the physical origin of the change in the fundamental mode and higher-order modes due to the refractive index and thickness of analyte. As a demonstration of an application and to test the limits of sensing, the substrates were used to image the surface functionalization using 2-nm-thick 11-mercaptoundecanoic acid and immobilization of 7-nm-thick mouse anti-human IgG antibody. In biological systems, where a priori knowledge about a process step is available, where accurate chemical composition testing is not necessary or possible, the presented method could be used to study the surface changes using a label-free sensing mechanism. © *2015 AIP Publishing LLC*. [http://dx.doi.org/10.1063/1.4937567]

I. INTRODUCTION

Plasmonic nanostructures have gained immense interest in the area of microscopy and spectroscopy because of the confinement of light at nanometer scale, very large field enhancement, and the possibility of surface plasmons (SP) excitation at normal incidence.[1–5] Moreover, inherent filtering nature of these nanostructures, resulting in color-selective transmission or reflection, has been used for applications in SP-based sensing.[6–8] It has been well studied that the wavelength corresponding to the SP excitation on plasmonic nanostructures is very sensitive to the small changes in the near-field refractive index and thickness of surrounding medium. In order to detect a very small amount of analyte, a very large sensitivity and a large signal-to-noise ratio are necessary. Extra ordinary transmission (EOT) phenomenon[9] utilizing sub-wavelength nano-aperture arrays is a good choice since the detection is based on transmission peaks against a dark background. However, EOT-based substrates in the visible region require precise nanofabrication techniques, since a small change from design parameters could shift the resonances by a large wavelength. Recent works for refractive index perturbation sensing utilize carefully fabricated EOT substrates to measure changes in

a)Electronic mail: ananthk@iitm.ac.in

resonance wavelength.[3,10] However, there are no reports on sample-to-sample variation of resonance wavelengths in the visible spectrum and the fabrication tolerances that are acceptable for commercial deployment. There are also no reports on same EOT substrates being used for sensing both thin (<10 nm) and thick dielectrics (>200 nm), since the phenomenon is inherently zeroth order phenomenon and extracting thickness information from EOT substrates using either spectral or colorimetric approach is not straightforward. For bio-chemical sensing applications, certain analytes like the functionalization agents or antibodies could be only a few nanometers thick[11] while certain protein molecule layers or viruses could be hundreds of nanometers thick,[12] and developing a universal approach for both these regimes is needed. Periodic plasmonic structures with period ≈ resonance wavelength in visible region are much easier to fabricate, but the optical signal corresponding to SP excitation that carries vital information about the surface is not captured either in transmission or reflection configuration, since the SP propagates along the surface of grating reliefs.[13] For this reason, fluorescently coupled leakage radiation microscopy has gained importance in the recent past,[14,15] wherein the information pertaining to SP is radiated out through the substrate and imaged. However, this approach requires fluorescent tagging of analytes to be used in a sensing experiment, which may not be desirable in certain cases, and the experiments are inherently narrow band due to the fluorescence phenomenon itself. A different approach to image sub-wavelength-thick analytes without fluorescent tagging is by using colorimetry, wherein films or regions of different refractive indices appear as distinctly different colors in an ordinary microscope. We describe a novel implementation of this approach by fabricating engineered plasmonic substrates and using microscopy configuration for real and Fourier plane (FP) imaging to capture surface changes at sub-wavelength thickness. We have recently shown that, by sandwiching a thin layer of homogeneous metal between the patterned metal and glass substrate, it is possible to convert the signature of SP from transmission dips to transmission peaks.[16,17]

In this work, we show that, in such substrates with a low aspect ratio and large period metallic gratings defined on a thin homogeneous metal-coated substrate exhibiting transmission resonances due to directional leakage of SP, the refractive index and thickness perturbations can be captured in the FP more accurately than in real plane. We systematically show that, apart from the fundamental SP mode, the higher-order Fabry-Perot modes (FPMs) are also hybrid in nature and also exhibit a 90° polarization rotation measured through leakage radiation. It was observed that, in a polarization microscopy setup, real-plane images of such substrates could be difficult to distinguish when coated with analytes, due to the small amounts of information arising from the direct zeroth order transmission, whereas, in the FP images, only the relevant SP-related information can be analyzed independently. Control experiments using different thicknesses of sub-wavelength-thick dielectric layers were systematically performed to image the evolution of the fundamental SP mode and higher-order FPMs in the Fourier plane. A

refractive index resolution of 10^{-5} was obtained from the analysis of the FP images. The presented method could be used for surface-sensing experiments involving changes in refractive index and/or thickness of the superstrate. Finally, to demonstrate a real bio-sensing application, the surface functionalization of the substrates using 2-nm-thick 11-mercaptoundecanoic acid and immobilization of 7-nm-thick mouse anti-human IgG antibody was imaged in the FP. We believe that our characterization approach is simple, involving only a tungsten halogen lamp, polarization optics, collecting lens, and camera for capturing minute changes on the surface.

II. CONTROL EXPERIMENT

A. Baseline spectral characteristics and spectral resolution of refractive index sensing

The cross-section schematic of the designed plasmonic structures is shown in Figure 1(a). The grating parameters were chosen based on broadband rigorous coupled wave analysis (RCWA), described in detail in our recent work.[16] The main objective for using such a substrate is to maximize the radiative leakage of SPs excited by the metal grating structures, resulting in a spectral transmission peak at resonance. The homogeneous metal layer serves two purposes: first, it acts as a mirror for most of the wavelengths, and second, for
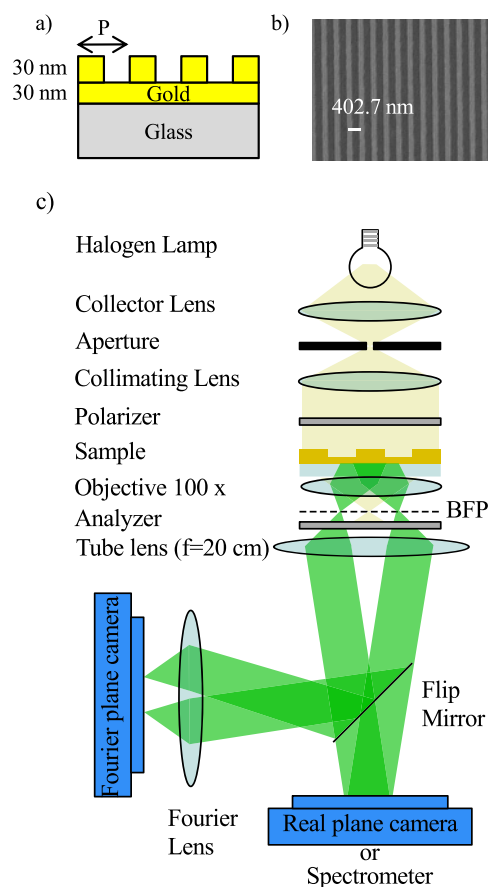

FIG. 1. (a) Schematic (not to scale) cross-section of 1D plasmonic structures on thin homogeneous metal-coated glass substrate. (b) SEM micrograph for fabricated structure of period 402.7 nm. (c) Characterization setup (not to scale).

the resonant wavelength that excites the SPs on top of the structure, due to the small thickness of the homogeneous metal layer, directional emission of the resonant wavelength due to leakage radiation occurs through the glass substrate. 1D and 2D periodic structures with periods P = 400 nm, 500 nm, and 600 nm were fabricated using e-beam lithography, gold evaporation, and lift-off process [however, the actual periods turned out to be 402.7 nm, 513.2 nm, and 607.1 nm due to fabrication tolerances]. The SEM micrograph of a fabricated 1D periodic structure with P = 402.7 nm and duty cycle = 0.44 is shown in Figure 1(b). The schematic diagram of characterization set up (not to scale) for real and FP imaging is shown in Figure 1(c). The samples were illuminated normally with a semi-collimated broadband visible light beam from a tungsten halogen source. A linear polarizer was positioned at an angle $\theta_P = 45°$ w.r.t. the grating vector to allow the components of both transverse electric (TE) and transverse magnetic (TM) polarizations to excite SP equally on the plasmonic structures. Due to the small thickness of the homogeneous metal (30 nm), at resonance wavelength, there occurs a radiative decay of the excited SPs through the substrate at specific angles dictated by the refractive index of the superstrate. Leakage of plasmon-coupled transmitted radiation from the bottom of the substrate was collected by a $100\times$ immersion oil objective lens of numerical aperture (N.A.) = 1.4. The light collected by the objective was passed through an analyzer positioned at an angle $\theta_A = 135°$ w.r.t the grating vector. Due to the anisotropic permittivity experienced by the light in these periodic structures, there occurs a differential phase retardation between the TE- and TM-coupled SP, and in these substrates, this leads to a polarization rotation of 90°. Details of the differential phase retardation and the polarization rotation phenomenon have been described in our recent work.[16] The transmitted light was then passed through a tube lens with a focal length of 20 cm and imaged using consumer-grade Sony charge coupled device (CCD) color camera with 1024×768 pixels and 5 μm pixel size to obtain real-plane images. A flip mirror was used to divert the beam to a Fourier lens, and an identical camera placed at its focus was used to obtain the FP images. In both the real-plane and Fourier-plane cameras, the near-infrared cut filter was removed, since the transparency of the filter was about $85\% \pm 6\%$ over the wavelength range of 400 nm to 635 nm, and at wavelengths higher than 645 nm, the transparency was lower than 20%. Since the wavelength range of the source was measured to be from 400 nm to 720 nm, and to make use of the entire visible region for colorimetric analysis, the infrared cut filter was removed. Prior to starting the experiments, the color calibration of the CCD cameras was performed using a simple white balance adjustment by imaging the beam without the fabricated samples in the optical path. Since the excitation in the experiment is inherently broadband, the individual color plane (R, G, or B) intensities were weighted using the image-capturing software for a fixed exposure time (0.4 s utilized throughout all experiments) at full intensity of the light source, such that the camera does not saturate and the histogram of the colors in the captured image is flat. Since, in the experiments, instead of absolute values of color, changes in the color from one superstrate to another were to be measured, this method was found to be simple and

provided consistent data across several sample images. No image manipulation was performed after the image captured in all the experiments.

For establishing a procedure for starting colorimetric sensing in control experiments, a thin layer of superstrate (PMMA 950 K used here) of thickness $t_s = 60$ nm was spin coated on the fabricated structure as illustrated in Figure 2(a). Figures 2(b) and 2(c) show the FP and real-plane images of PMMA-coated structure of $t_s = 0$ nm (no PMMA, only air) and $t_s = 60$ nm for period P = 402.7 nm at $\theta_P = 45°$ and $\theta_A = 135°$, respectively. The cross-axis arrangement of polarizer and analyzer ($\theta_P - \theta_A = \pm 90°$) almost diminished the direct transmission of light [weak central spot in FP images shown in Figure 2(b-i)] through the fabricated
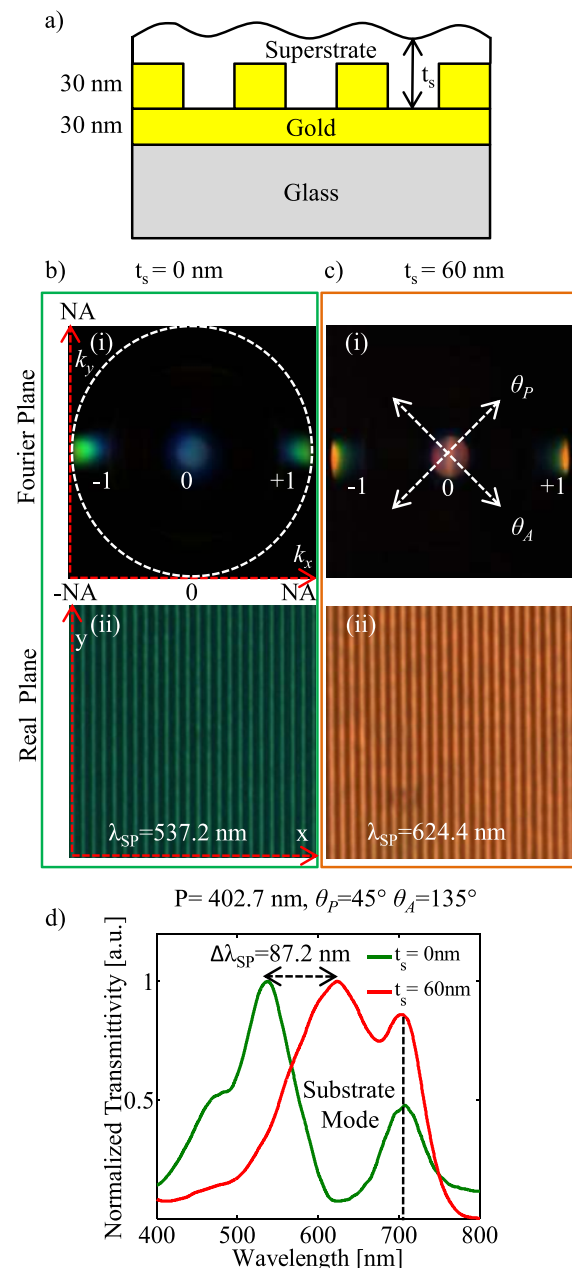

FIG. 2. (a) Schematic (not to scale) cross-section of 1D plasmonic structures coated with superstrate; FP and real-plane images of structures with (b) $t_s = 0$ nm and (c) $t_s = 60$ nm. (d) Experimental spectra.

structures. This allowed the camera to capture SP-related momentum information against a dark background with -1 and $+1$ orders of the transmitted light [left- and right-hand side spots in Fig. 2(b-i)] of green color. In the case of PMMA-coated structure, bright ± 1 order emissions of orange color were imaged as shown in Figure 2(c-i). To verify the variation in color of the captured images, the real-plane imaging camera was replaced with a spectrometer, with total intensity of transmitted light projected into the sensor, and the experimental spectra for these structures were obtained as shown in Figure 2(d). The experimental peak position was found to be at 537.2 nm for structure with $t_s = 0$ nm, which is attributed to the SP excitation at the interface of periodic metal structures and air. An additional peak of smaller magnitude can be observed at 708.9 nm, which is attributed to the excitation of SP at the interface of glass substrate and homogeneous metal, which was verified by electric fields calculated using simulations [not shown here]. The peak position for $t_s = 60$ nm was found to be at 624.4 nm, which is corresponding to the SP excitation at the interface between periodic metal structures and PMMA. The shift in the peak position was attributed to the change in the refractive index from air (n = 1) to PMMA (n = 1.489). The sensitivity from experimental spectra was calculated to be 179 nm/RIU for the 60-nm-thick layer. The peak position corresponding to the excitation of SP at the interface of glass substrate and homogeneous metal was found to be almost the same for both the cases, which ensures the independence from changing the refractive index of superstrate.

B. Refractive index sensing using Fourier plane colorimetry and comparison with real-plane colorimetry

The change in color from green to orange was clearly observed with the variation in refractive index in real-plane and FP images. To measure the repeatability, several patterns on a substrate and 3 different substrates containing similar patterns were imaged in the real and Fourier planes. This was performed to establish the threshold level of black background in the FP images. In all of the cases, the maximum values of red (R), green (G), and blue (B) were found to be less than 5 (maximum being 255) in FP images and, hence, that was chosen as the threshold level above which all information would be considered for sensing purposes. For the rest of the work, the threshold background levels were maintained the same for consistency. It can be noticed from Figures 2(b-i) and 2(c-i) that there exists a weak central spot in the FP images due to the direct (0th) transmission that actually changes with the superstrate. While, for sensing purposes, any information or every piece of information is crucial, the direct transmission actually varies depending on the transmission characteristics of polarizer itself, the relative positioning of the polarizer and analyzer, condensing optics. However, for these structures, the direct transmission does not arise from coupling to SPs since, in our structures, only ± 1 orders couple to SPs with a measured coupling efficiency of 12%. Hence, comparing this information directly between $t_s = 0$ nm and $t_s = 60$ nm was rather inconsistent,

and to ensure that only the SP-related information was used for the sensitivity analysis, the central spot was omitted and replaced with the measured threshold level. It is, however, possible to overcome this problem by employing a spatial filter in the back focal plane of the objective by using a transparency mask that blocks the central spot and allows all other information to pass through. In the presented experiments, this was not performed since the access to the back focal plane of the objective was restricted, due to the presence of the analyzer and positioners, very close to the back focal plane. Next, the regions having R or G or B above the threshold were extracted using a simple program, thus retaining information only about the ± 1 orders corresponding to the SP mode. Then, the mean values of R, G, and B were directly calculated for both the left side and right side spots independently. The separate calculation was deemed necessary as a slight asymmetry in the intensity between the left- and right-side spots in the images could be possible due to placement of substrates on the microscope stage. While, to a large extent, the asymmetry could be reduced a lot just by adjusting the position of the substrate, for the purpose of accuracy, separate calculations were performed. In order to increase the range of measurement, the images were also converted to cyan (C), magenta (M), yellow (Y), and black (K) and the mean values of each of these components were calculated for each of the spots. Due to the presence of 4 planes, namely, C, M, Y, and K, each ranging from 0 to 255, instead of R, G, and B, the range of the measurement can be improved considerably. Next, the mean values of R, G, and B and C, M, Y, and K were calculated for the same sample coated with PMMA, with similar positioning on the stage. The mean values of R, G, and B and C, M, Y, and K of the left-side spot, before and after PMMA coating, are plotted from FP images in Figure 3(a), while the values in Figure 3(b) correspond to the mean value obtained by direct calculation of the mean in the field of view of the microscope. In other words, Figure 3(b) includes the effect of the direct
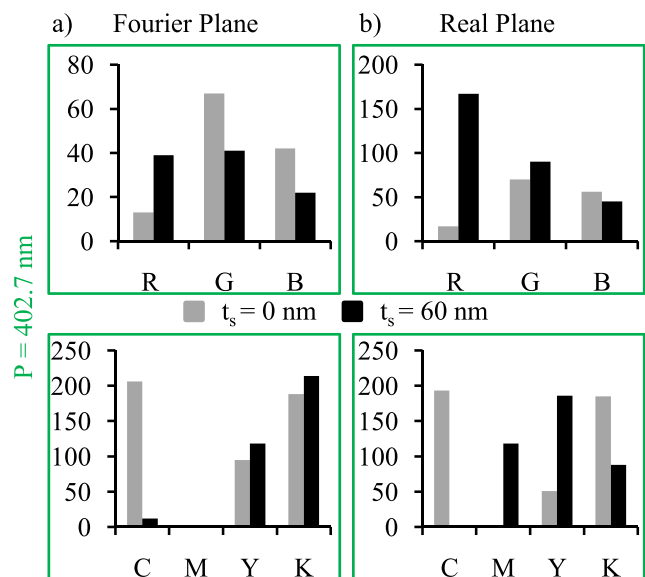

FIG. 3. Average values of R, G, and B and C, M, Y, and K for (a) Fourier plane and (b) real-plane images.

transmission also. It will be shown later in this work as to why this could be difficult to analyze in certain cases. From Figures 3(a) and 3(b), the value of R changed from 13 to 39 and 17 to 167, respectively, over the refractive index change (Δn) of 0.489 for FP and real images. For the CMYK model, the value of Y changed by 23 and 135 for the same refractive index variation. The changes in the values of [C, M, Y, K] (ΔC, ΔM, ΔY, ΔK) were computed. Using the standard deviation (σ) value calculated from the repeatability measurements [$\sigma_{CMYK} = 2.05$ for FP images and $\sigma_{CMYK} = 3.77$ for real images], the refractive index resolution can be defined as[18]

$$\text{Index Resolution} = \left(\frac{\Delta n}{\Delta C^2 + \Delta M^2 + \Delta Y^2 + \Delta K^2} \right) \times 2\sigma. \tag{1}$$

Using Eq. (1) for 60-nm-thick PMMA layer, the value of $\Delta C^2 + \Delta M^2 + \Delta Y^2 + \Delta K^2$ was calculated to be 38 841 and the refractive index resolution was calculated to be 5.16×10^{-5} RIU and 4.67×10^{-5} RIU in the FP and real images. In the real image, the larger variation of Y component was contributed because of the 0th diffraction order along with ± 1 orders of orange color for $t_s = 60$ nm as shown in Figure 2(c-i). In Figure 2(b-i), the same 0th order appeared as a very weak central spot for $t_s = 0$ nm. FP images with ± 1 orders corresponding only to transmission plasmonic resonances are a good choice to quantify the surface changes, since the real-plane images include the effect of 0th order that may or may not be indicative of surface perturbations. There exists a limitation in this approach based on FP analysis, however, that, in the case of superstrate patterned on a very small spatial region of the field of view of the microscope, the shift in SP resonance cannot be observed in FP images or experimental spectra due to the large background appearing from uncoated/unpatterned region. Figure 4(a) shows a section of the obtained real-plane image of a square region of 15 μm $\times$ 15 μm consisting of PMMA of 60-nm thickness, while the green regions contain no PMMA when the field of view was 150 μm $\times$ 150 μm. In such cases, the FP image largely consists of information of the background green color spots and very small content of orange color appear upon higher exposure times of the camera. Though this is a limitation from FP-based sensing, these substrates do provide a high
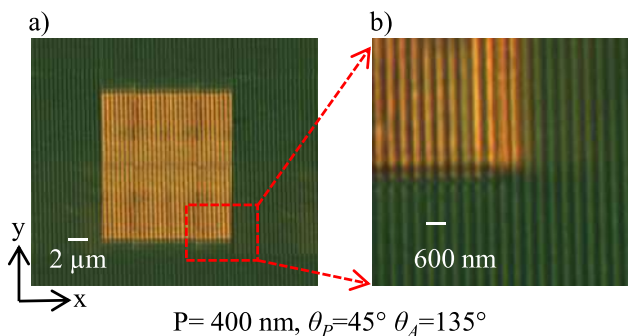

FIG. 4. (a) Real-plane image with PMMA patterned on 1D plasmonic structure and (b) zoomed-in region of real-plane image for P = 402.7 nm at $\theta_P = 45°$ and $\theta_A = 135°$.

color contrast in the real plane for studying spatial morphology perturbations. In such cases, the real-plane image content may be analyzed provided the images could be registered spatially and the thickness and the index of the superstrate is already known, which is probably not the case in real experiments. Of course, this problem may be overcome by collecting the information pertaining to a patterned region using a pin hole in the image plane and further using only this light for Fourier analysis using additional lenses. However, this may not be a practical approach, since, in real samples, the patterned regions need not be defined lithographically and thus can vary in size from one to another. Secondly, since this approach is based on diffraction-based coupling, care must be taken to ensure that sufficient number of periods of the grating structures are actually covered by the analyte, as otherwise, there could be errors due to change in colors due to the same analyte covering different number of grating periods.

C. Thickness sensing using FP colorimetry and momentum information, using hybridicity of fundamental SP and higher-order modes

To capture the effect of thickness of a homogeneous superstrate, four different t_s (60 nm, 160 nm, 270 nm, and 620 nm) of PMMA 950 K were spin coated on the fabricated structures. Different thicknesses of the superstrate were verified by confocal microscope and profilometer measurements over several samples. Figures 5(a) and 5(b) show the FP and real-plane images of PMMA-coated structures with period P = 513.2 nm, for various superstrate thicknesses, at $\theta_P = 45°$ and $\theta_A = 135°$, respectively. When these structures were illuminated by the broadband source, leakage radiation of SP gave rise to FP images corresponding to single ± 1 emission as shown in Figures 5(a-i) and 5(a-ii) or multiple bright ± 1 order emissions of different colors shown in Figures 5(a-iii)–5(a-v). In the FP images, we observed that the number of colors emitted depends on the thickness of the superstrate. In Figure 5(a-i), bright ± 1 order emission of yellow color was observed, which is attributed to fundamental SP mode excited at grating/air interface, whereas, for the case of $t_s = 60$ nm, the emission of red color was observed as shown in Figure 5(a-ii) attributed to fundamental SP mode excited at grating/PMMA superstrate interface. This change in color from yellow to red was observed due to the change in refractive index from air to superstrate (PMMA). As the thickness of superstrate increased to 160 nm, bright ± 1 order of two distinct emissions, one of red color (less intensity on outer portion of the image) and another of yellow color (high intensity on inner portion), were observed. The outermost red color emission was attributed to hybrid nature fundamental SP mode, and the inner yellow color emission was attributed to the first higher-order hybrid Fabry Perot mode (FPM) [confirmed later with simulations in this paper]. In the case of 270-nm-thick superstrate, presence of higher-order FPMs and fundamental SP mode was imaged with bright ± 1 order emissions of green, orange, and red color [with lesser intensity at outermost portion]. Whereas, in the case of 620-nm-thick superstrate, presence of higher-order FPMs and fundamental SP mode was imaged with bright ± 1 order emissions of green, orange, and red color and a deep red
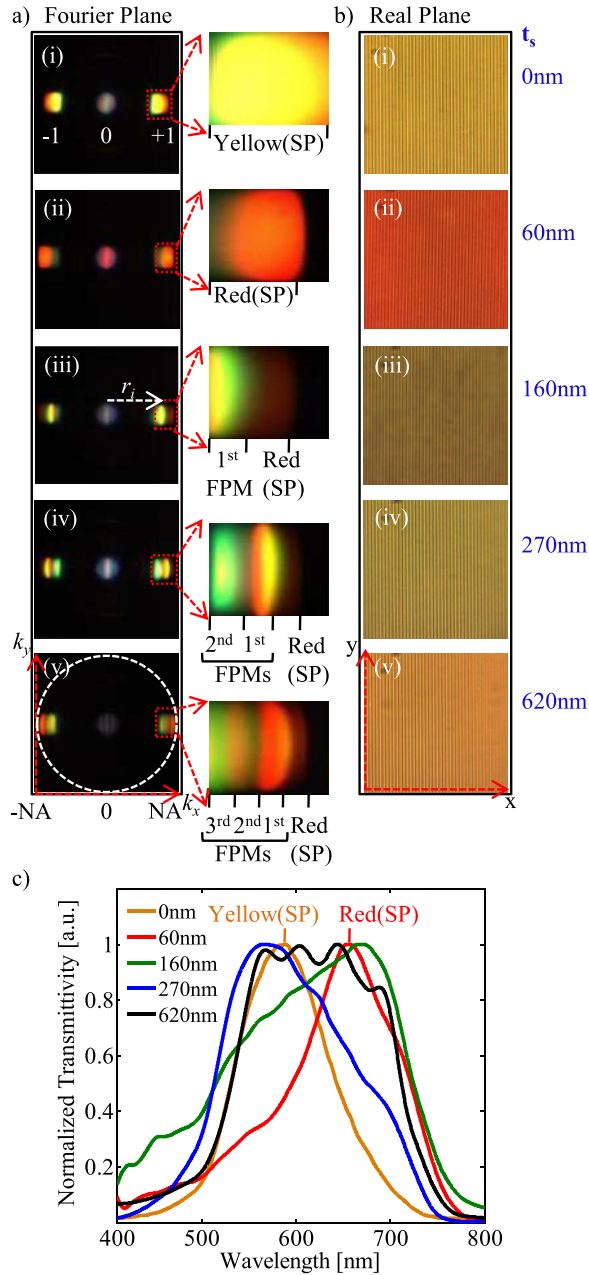
a) Fourier Plane   b) Real Plane

FIG. 5. (a) FP images. (b) Real-plane images. (c) Experimental spectra of PMMA-coated 1D plasmonic structure for $P = 513.2\,nm$ with different t_s at $\theta_P = 45°$ and $\theta_A = 135°$.

the fundamental SP mode has the highest absorption due to very high interaction with the metal layer, while the higher-order FPMs usually interact much lesser with the metal layer, hence suffering lower losses. For a fixed exposure time of the camera, it might appear that, in certain cases, the fundamental SP mode is slightly bigger and, in certain other cases, the FPMs are bigger. These are largely governed by the sensitivity of the CCD sensor and the pixel-to-pixel cross-talk in the detection electronics. Hence, all the experiments were performed when the objective is positioned so that the bottom patterned grating structure remains in focus in the real plane. The average size of the each of the fundamental SP mode spots in the FP images in our experiments was about $50\,\mu m$; however, this can vary depending upon the magnification of the Fourier lens used to image.

In order to capture the properties of each of these colored spots, a line was drawn from the center of the FP image to the mid-point of each colored emission 'i' as shown in Figure 5(a-iii). Since the images are in the reciprocal space, the images actually represent the momentum or effective index information directly. The line joining the center of the image to the corresponding i^{th} emission has a distance r_i [where $i = 1$, 2, and 3, corresponding to the emission color]. All the FP images were formed over a very weak circular background of radius ($r_{circ} > r_i$), corresponding to the maximum collection angle of leakage radiation for the high NA objective lens. The effective refractive index (n_{eff}) corresponding to the guided modes can be determined directly from the radii of orders with different colors in the FP image using the expression

$$n_{eff} = \left(\frac{r_i}{r_{circ}} \times (NA - 1) \right) + 1. \qquad (2)$$

Conversion from radii to n_{eff} using Eq. (2) yields n_{eff} of 1.316 for 5(b); 1.289 and 1.338 for 5(c); 1.275, 1.321, and 1.363 for 5(d); and 1.283, 1.318, 1.346, and 1.373 for 5(e), respectively. An added advantage of this FP imaging over real-plane imaging is that the effective refractive index of guided modes could be easily calculated. However, the sensitivity calculated from only using the separation distance r_i, was very low as the change in the effective refractive index from one particular superstrate thickness to another (specifically 0 nm to 60 nm) is very small (the distance of the spots from the center varied no more than ten pixels across these two cases), whereas the sensitivity using colorimetry for the same case is high as the color changes from yellow to red as shown in Figs. 5(a-i) and 5(a-ii), respectively. Rather than using only the position of the spots for extracting this information, it is beneficial to consider the color changes along with the position, since the changes for a small-index perturbation are very large in the color of the spots.

To verify the presence of FPMs with the increase in PMMA thickness, the experimental spectra for different thicknesses of PMMA were obtained as shown in Figure 5(c). The peak at $\lambda_{SP} = 588.2\,nm$ for $t_s = 0\,nm$ was attributed to fundamental SP mode excited on grating/air interface, whereas the peak at $\lambda_{SP} = 655.2\,nm$ for $t_s = 60\,nm$ was attributed to fundamental SP mode excited on grating/PMMA interface. The

color [with lesser intensity at outermost portion]. The presence of yellow color in Figure 5(a-iii); green and orange in Figure 5(a-iv); and green, orange, and red in Figure 5(a-v) attributed to FPMs confirms an increase in number of higher-order modes with increasing thickness of the superstrate. In these FP images, a slight asymmetry in [+1, 0] and [−1, 0] was observed because of the small tilt of the sample w.r.t. plane of incidence, due to positioning issues. The exposure time for the camera while capturing the images was kept fixed throughout the experiments. It can also be observed that, apart from the color and the position, the size of the spots change even under tight focus conditions as the thickness of the analyte changes. This is attributed to the change in the Q factors of resonance due to loading with a dielectric and also due to the fact that

shift in λ_{SP} with change in refractive index was observed with change in color from yellow to red in FP images as shown in Figures 5(a-i) and 5(a-ii). The occurrence of substrate mode for P = 513.2 nm was not in this wavelength range. So the peaks shown in Figure 5(c) are attributed to SP excitation only. The presence of higher-order FPMs was noticed with increase in thickness of PMMA, but it is very difficult to extract the correct information regarding the thickness since the peaks attributed to higher-order modes are not sharp enough. The transmittivity value of higher-order FPMs was found to be more than the fundamental SP mode with increase in PMMA thickness since higher-order modes propagate with the majority of the field away from metal-dielectric interface, resulting in low absorption due to weaker interaction with metal. This is the reason the intensity of the red color attributed to fundamental SP mode was decreasing continuously with increase in PMMA thickness, whereas the colors attributed to FPMs were more intense in FP images shown in Figure 5(a). The change in color from yellow to red in Figures 5(b-i) and 5(b-ii) can be clearly noticed. But as the thickness t_s increases, the information related to presence of different FPMs cannot be seen in real images. The color of the real image for $t_s = 0$ nm shown in Figure 5(b-i) looks similar to the color for $t_s = 270$ nm. Only from FP images can one detect that a large perturbation of refractive index and thickness has occurred. In other words, FP imaging is the best option for refractive index and thickness sensing, since the emitted color of fundamental SP can be used to measure the changes in refractive index and the number of excited FPMs can be used to measure the changes in thickness. The main advantage of proposed plasmonic substrates and imaging technique over EOT substrates is imaging of higher-order modes as different colored emissions with increase in superstrate thickness. In EOT substrates, since *0th* order is responsible for SP excitation, the imaging of higher-order modes is not possible.

We further confirmed the influence of the superstrate thickness on the transmittivity of the structures using RCWA method. Figure 6(a) shows the simulated transmittivity map for different PMMA thickness w.r.t. wavelength. The wavelength position of fundamental SP mode is essentially constant for PMMA thickness larger than 250 nm. The number and wavelength position of FPMs varied with PMMA layer thickness. In other words, above 250 nm PMMA thickness, the changes in wavelength positions will occur only for higher-order FPMs while the fundamental SP mode will be independent of the thickness variation. The presence of three FPMs, superstrate SP mode, and substrate SP mode can be clearly seen in Figure 6(a). To quantify the changes in color for fundamental SP mode and higher-order FPMs due to the variation in thickness, we compared the FP images corresponding to $t_s = 270$ nm and $t_s = 620$ nm as shown in Figures 5(a-iv) and 5(a-v), respectively. The changes in [R, G, B] and [C, M, Y, K] values for fundamental SP mode imaged as deep red color as shown in Figures 5(a-iv) and 5(a-v) were [$\Delta R^2 = 2^2 + \Delta G^2 = 2^2 + \Delta B^2 = 1^2$] = 9 and [$\Delta C^2 = 0^2 + \Delta M^2 = 9^2 + \Delta Y^2 = 3^2 + \Delta K^2 = 2^2$] = 94 were almost negligible (background threshold $R < 5$, $G < 5$, and $B < 5$) for increasing the thickness from 270 nm to 620 nm, which justifies the statement that the
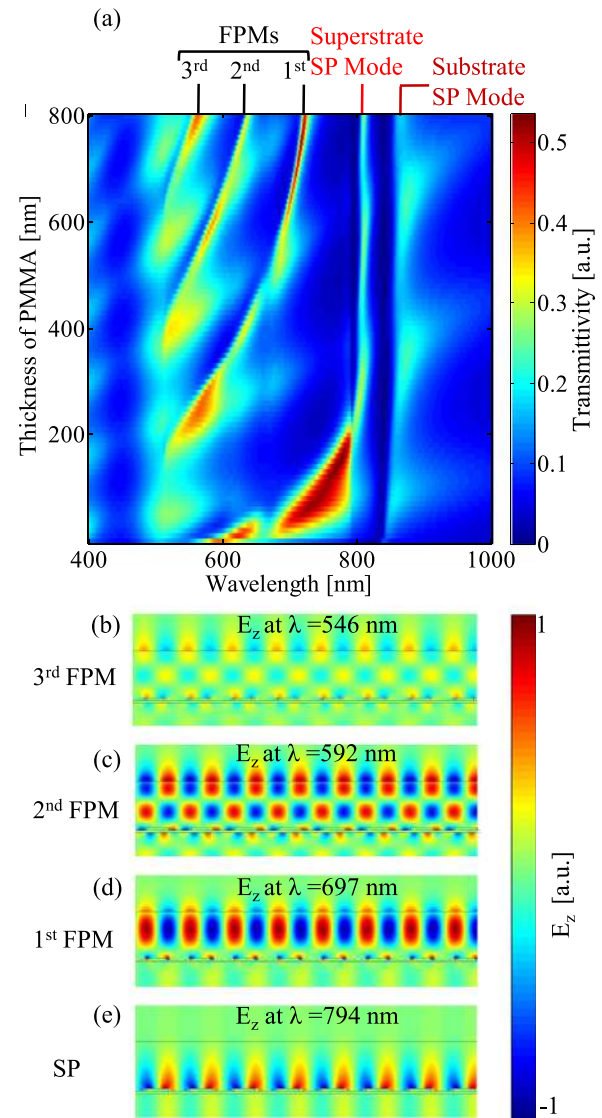

FIG. 6. (a) Simulated transmittivity map for different PMMA thicknesses; E_z distribution, (b) $\lambda = 546$ nm, (c) $\lambda = 592$ nm, (d) $\lambda = 697$ nm, and (c) $\lambda = 794$ nm for $t_s = 620$ nm.

wavelength position of fundamental SP mode is independent for PMMA thickness larger than 250 nm. For higher-order FPMs, an appreciable change in [R, G, B] and [C, M, Y, K] values [$\Delta R^2 = 24^2 + \Delta G^2 = 79^2 + \Delta B^2 = 35^2$] = 8042 and [$\Delta C^2 = 24^2 + \Delta M^2 = 77^2 + \Delta Y^2 = 42^2 + \Delta K^2 = 40^2$] = 9869 was observed over the same thickness change of 270 nm. So the changes in [R, G, B] and [C, M, Y, K] values for higher-order FPMs captured in FP images can be used to measure the variation in thickness of superstrate.

To ensure the presence of higher-order FPMs, the electric field E_z was calculated for resonance wavelengths obtained from simulated transmission spectrum of PMMA for $t_s = 620$ nm as shown in Figures 6(b)–6(e). E_z distribution in Figure 6(e) is attributed to excitation of fundamental SP mode at patterned metal/PMMA interface. From the field plots shown in Figures 6(b)–6(d), the excitation of FPMs was confirmed. The metal/PMMA/air structure corresponds to a waveguide with cladding layers formed by metal at the bottom and air on the top, while the guiding layer is formed by the

PMMA. It was clear that three FPMs could exist for $t_s = 620$ nm of PMMA, which was found to be in a good agreement with captured FP image discussed in Figure 5(a-v).

D. FP colorimetry in 2D structures and simultaneous multiwavelength-resonance-tracking-based sensing

To confirm the methodology, we repeated the same experiment with 2D plasmonic structures. The SEM micrograph of a fabricated 2D plasmonic structure is shown in Figure 7(a). Different thicknesses of PMMA 950 K were spin coated on the fabricated 2D structures similar to experiments performed with 1D plasmonic structures. Figures 7(b)–7(d) show the FP images of PMMA-coated structure with different thicknesses for period $P_x = 505.2$ nm, $P_y = 508.3$ nm at $\theta_P = 45°$ and $\theta_A = 135°$, respectively.

In the FP images shown in Figure 7, the bright emission of colors attributed to SP excitation was found to be both in horizontal and vertical directions due to periodicity in both x and y directions. In Figure 7(b), the bright [±1, 0] and [0, ±1] order emission of yellow color was observed, which attributed to fundamental SP mode excited at metallic pillars and air interface, whereas, for the case of $t_s = 60$-nm-thick PMMA, the emission of red color was observed attributed to fundamental SP mode excited at metallic pillars and PMMA interface as shown in Figure 7(c). The same yellow color emission for *1st* FPM mode was observed with increase in thickness of PMMA to 160 nm as observed in 1D plasmonic structures. This confirms that number of emission of colors
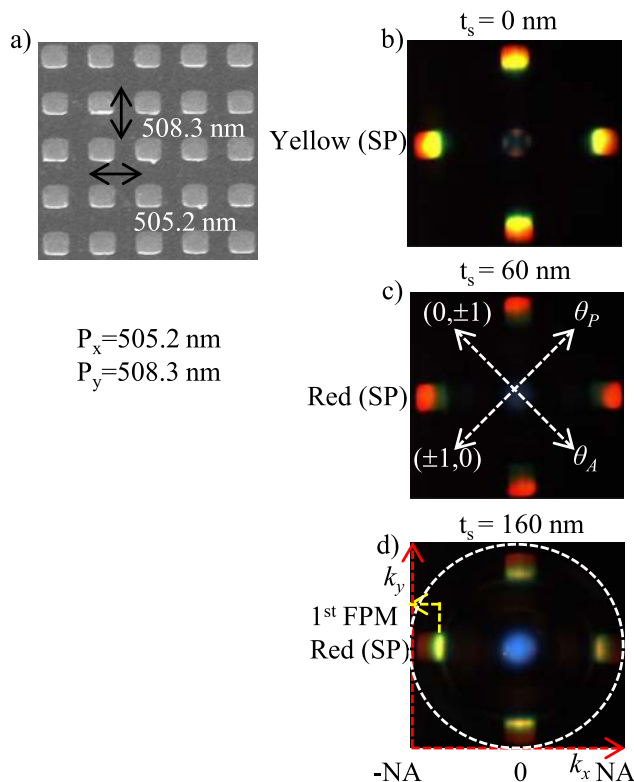
attributed to higher-order FPMs captured in FP images can be used as a coarse method for thickness sensing of dielectric films.

2D rectangular pillars with different periodicity in x and y directions ($P_x = 505.2$ nm, $P_y = 403.4$ nm) were fabricated and used for sensing. Figure 8(a) shows the SEM micrograph for $P_x = 505.2$ nm and $P_y = 403.4$ nm. As a result of which, yellow-colored [±1, 0] order and green-colored [0, ±1] order were observed in $\theta_P = 45°$ and $\theta_A = 135°$ cross-axis arrangement for $P_x = 505.2$ nm and $P_y = 403.4$ nm as shown in Figure 8(b). For the case of $t_s = 60$ nm, the emission of red-colored [±1, 0] order and orange-colored [0, ±1] order were observed and attributed to the fundamental SP mode excited at metallic pillar and PMMA interface as shown in Figure 8(c). The refractive index resolution was achieved as 4.39×10^{-5} RIU for emission of red-colored [±1, 0] order of metallic pillars with $P_x = 505.2$ nm and 7.04×10^{-5} RIU for orange-colored [0, ±1] order of metallic pillars with $P_y = 403.4$ nm using the CMYK model. Structures like these exhibiting multiple resonances due to different periodicities in different directions could find potential applications in imaging sensors, wherein characteristics of analytes coated on the structure at different wavelengths could be extracted in a single experiment.

III. APPLICATION TO BIO-SENSING DETECTION OF SURFACE FUNCTIONALIZATION AND IMMOBILIZATION OF ANTIBODY

To verify the usability of fabricated plasmonic substrates for biological applications, substrates were incubated in 5 ml ethanol solution containing 1 mM concentration of 11-mercaptoundecanoic acid[19] (11-MUA) for 12 h.

FIG. 7. (a) SEM micrograph; FP images of PMMA-coated 2D plasmonic structure for $P_x = 505.2$ nm, $P_y = 508.3$ nm at $\theta_P = 45°$ and $\theta_A = 135°$ for t_s (b) 0 nm, (c) 60 nm, and (d) 160 nm.
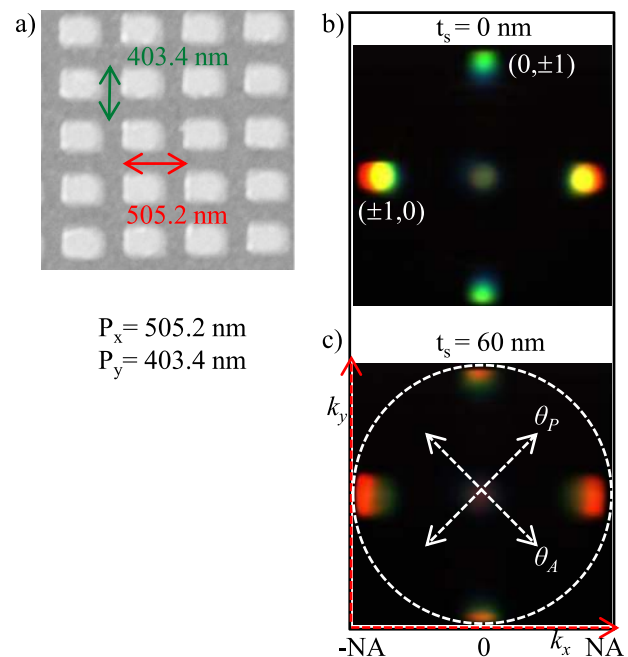
FIG. 8. (a) SEM micrograph; FP image of PMMA-coated 2D plasmonic structure with rectangular pillars for $P_x = 505.2$ nm, $P_y = 403.4$ nm at $\theta_P = 45°$ and $\theta_A = 135°$ for t_s (b) 0 nm and (c) 60 nm.

Subsequently, the samples were washed in ethanol and DI water. The thickness of 11-MUA deposited on substrates was found to be 2.1 nm $\pm$ 0.20 nm using ellipsometer. The sample was characterized using the same setup as in Figure 1(c). Figures 9(a) and 9(b) show the FP and real-plane images captured with air and 11-MUA-coated 1D plasmonic structures with P = 402.7 nm. In the case of FP image with air superstrate as shown in Figure 9(a-i), the bright emission of green color that is attributed to the fundamental SP mode excitation on metallic pattern and air interface was imaged [discussed earlier]. Figure 9(b-i) shows the structures with 11-MUA coated on them. The same red shift in color was also observed in real-plane images shown in Figures 9(a-ii) and 9(b-ii), which was confirmed with a SP shift to longer wavelength by 13 nm from experimental spectra. The average values of the individual C, M, Y, and K for captured images are shown in Figures 10(a) and 10(b). The value of Y changed from 95 to 114 and 51 to 83 for FP and real-plane images, respectively, due to both refractive-index-(n = 1 to 1.36) and thickness (0 to 2.1 nm)-induced surface modifications after depositing 11-MUA. The structure coated with

FIG. 10. Average values of C, M, Y, and K for P = 402.7 nm, (a) Fourier plane and (b) real-plane images; average values of C, M, Y, and K for P = 513.2 nm, (c) Fourier plane and (d) real-plane images.

11-MUA was found to be darker because of a peak optical absorption[20] in the wavelength range of 520–720 nm.

After 11-MUA coating, a mouse anti-human IgG (antibody) was immobilized with thickness 7.2 nm $\pm$ 0.50 nm using the procedure described in a recent work,[21] on top of the plasmonic substrates, and the FP and real-plane images were captured as shown in Figures 9(c-i) and 9(c-ii). The change in average values of C, M, Y, and K shown in Figures 10(a) and 10(b) reveals the surface modification due to the presence of IgG. Since the refractive index for 11-MUA and IgG is almost the same, the change in value of Y is lesser in case of IgG compared to the 11-MUA layer due to a mere thickness-induced surface modification. The real-plane images have the effect of 0th order also, so FP images are a good choice to distinguish between refractive-index-induced surface change and a mere thickness-induced surface change.

Figures 9(d)–9(f) show the FP and real-plane images captured for air-, 11-MUA-, and IgG-coated 1D plasmonic structures with P = 513.2 nm. The change in color can be clearly seen in both FP and real images with naked eyes. The average values of the individual C, M, Y, and K for captured images are shown in Figures 10(c) and 10(d), which confirm the surface modification due to the presence of 11-MUA and IgG. FP imaging of proposed engineered substrates with colorimetric capability could be used for biochemical attachment sensing.

IV. CONCLUSION

We demonstrated colorimetric sensing using FP imaging of SP, where the excitation of hybrid nature fundamental SP mode and hybrid higher-order FPMs was used to provide ultra-sensitive response to the changes in refractive index and thickness of sub-wavelength thin films coated on 1D and 2D periodic plasmonic structures. The change in bright

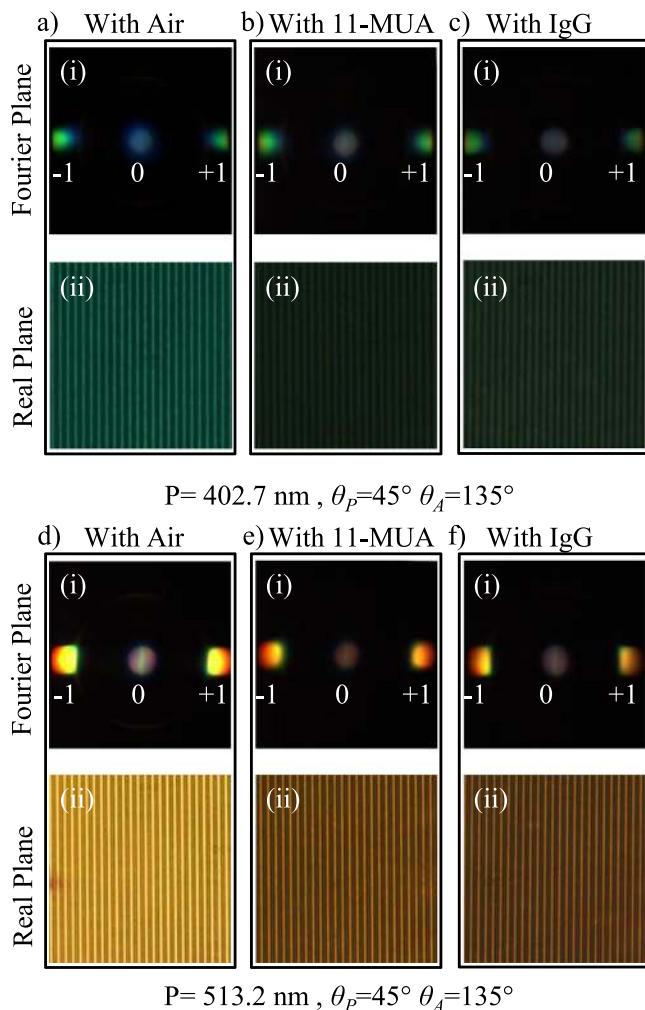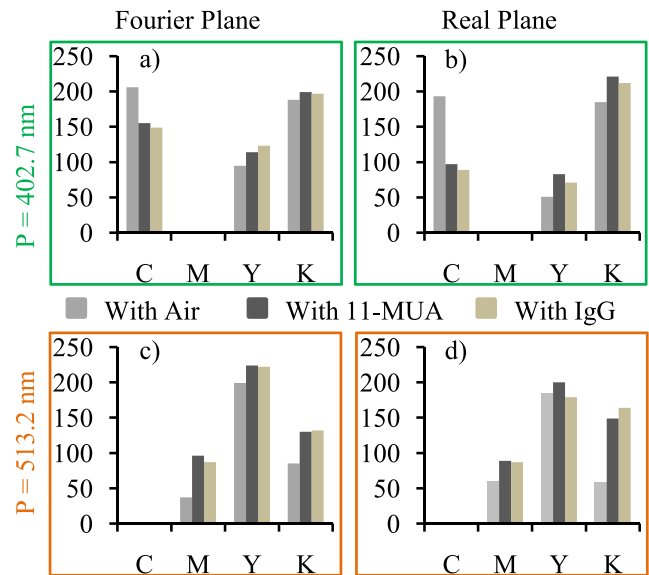
FIG. 9. FP and real-plane images (a) with air, (b) with 11-MUA, and (c) with IgG for 1D structure of P = 402.7 nm and (d) with air, (e) with 11-MUA, and (f) with IgG for 1D structure of P = 513.2 nm at $\theta_P = 45°$ and $\theta_A = 135°$.

emitted color of fundamental SP against a dark background was used to measure the changes in refractive index of sub-wavelength dielectric films, and the number of excited higher-order FPMs captured in FP images was used to analyze the changes in thickness. FP imaging was found to be more attractive compared to real-plane imaging since both refractive-index- and thickness-related information can be extracted from FP images. The proposed FP imaging for colorimetric sensing is a promising tool for biochemical attachment sensing using only an imaging camera, a cross polarizer-analyzer arrangement, and engineered low-aspect-ratio plasmonic substrates. With successful integration of these plasmonic substrates with microfluidics, a real-time monitoring of biochemical reactions could be possible.

ACKNOWLEDGMENTS

[1]J. P. Camden, J. A. Dieringer, J. Zhao, and R. P. Van Duyne, Acc. Chem. Res. **41**, 1653 (2008).

[2]Q. Sun, K. Ueno, H. Yu, A. Kubo, Y. Matsuo, and H. Misawa, Light: Sci. Appl. **2**, e118 (2013).

[3]A. E. Cetin, A. F. Coskun, B. C. Galarreta, M. Huang, D. Herman, A. Ozcan, and H. Altug, Light: Sci. Appl. **3**, e122 (2014).

[4]R. Vogelgesang, J. Dorfmüller, R. Esteban, R. T. Weitz, A. Dmitriev, and K. Kern, Phys. Status Solidi B **245**, 2255 (2008).

[5]M. W. Knight, J. Fan, F. Capasso, and N. J. Halas, Opt. express **18**, 2579 (2010).

[6]B. Zeng, Y. Gao, and F. J. Bartoli, Sci. Rep. **3**, 2840 (2013).

[7]M. E. Stewart, C. R. Anderton, L. B. Thompson, J. Maria, S. K. Gray, J. A. Rogers, and R. G. Nuzzo, Chem. Rev. **108**, 494 (2008).

[8]S. Yokogawa, S. P. Burgos, and H. A. Atwater, Nano Lett. **12**, 4349 (2012).

[9]T. W. Ebbesen, H. Lezec, H. Ghaemi, T. Thio, and P. Wolff, Nature **391**, 667 (1998).

[10]D. Jones, N. Liu, B. Corbett, P. Lovera, A. Quinn, and A. O'Riordan, J. Phys.: Conf. Ser. **307**, 012005 (2011).

[11]D. Saerens, L. Huang, K. Bonroy, and S. Muyldermans, Sensors **8**, 4669 (2008).

[12]Y. Vashpanov, J. Young Son, and K. Dal Kwack, Sensors **8**, 6225 (2008).

[13]L. Feng, Z. Liu, and Y. Fainman, Appl. Opt. **50**, G1 (2011).

[14]A. Krishnan, S. Frisbie, L. G. de Peralta, and A. Bernussi, Appl. Phys. Lett. **96**, 111104 (2010).

[15]S. Frisbie, C. Chesnutt, M. Holtz, A. Krishnan, L. G. De Peralta, and A. Bernussi, IEEE Photonics J. **1**, 153 (2009).

[16]P. Arora and A. Krishnan, J. Lightwave Technol. **32**, 4816 (2014).

[17]P. Arora and A. Krishnan, in *Proceedings of PIERS* (2013), pp. 927–931.

[18]M. Khorasaninejad, S. M. Raeis-Zadeh, H. Amarloo, N. Abedzadeh, S. Safavi-Naeini, and S. S. Saini, Nanotechnology **24**, 355501 (2013).

[19]J. C. Love, L. A. Estroff, J. K. Kriebel, R. G. Nuzzo, and G. M. Whitesides, Chem. Rev. **105**, 1103 (2005).

[20]Y. Guo, Z. Wang, H. Shao, and X. Jiang, Analyst **137**, 301 (2012).

[21]P. Bhadra, M. Shajahan, E. Bhattacharya, and A. Chadha, RSC Adv. **5**, 80480 (2015).